Colloids and Surfaces B: Biointerfaces 75 (2010) 425–431

Contents lists available at ScienceDirect

Colloids and Surfaces B: Biointerfaces

journal homepage: www.elsevier.com/locate/colsurfb

Using flowerlike polymer–copper nanostructure composite and novel organic–inorganic hybrid material to construct an amperometric biosensor for hydrogen peroxide

Jinfen Wang, Ruo Yuan*, Yaqin Chai, Wenjuan Li, Ping Fu, Ligen Min

Key Laboratory on Luminescence and Real-Time Analysis, Ministry of Education, College of Chemistry and Chemical Engineering, Southwest University, Chongqing 400715, China

ARTICLE INFO

Article history:
Received 26 May 2009
Received in revised form 8 September 2009
Accepted 14 September 2009
Available online 22 September 2009

Keywords:
Flowerlike copper–polymer nanostructure
Zirconia–chitosan sol–gel
Au nanoparticles
Horseradish peroxidase
Hydrogen peroxide biosensor

ABSTRACT

A new type of amperometric hydrogen peroxide biosensor was fabricated by entrapping horseradish peroxidase (HRP) in the organic–inorganic hybrid material composed of zirconia–chitosan sol–gel and Au nanoparticles (ZrO_2–CS–AuNPs). The sensitivity of the biosensor was enhanced by a flowerlike polymer–copper nanostructure composite (pPA–FCu) which was prepared from co-electrodeposition of $CuSO_4$ solution and 2,6-pyridinediamine solution. Several techniques, including UV–vis absorption spectroscopy, scanning electron microscopy, cyclic voltammetry, chronoamperometry and electrochemical impedance spectroscopy were employed to characterize the assembly process and performance of the biosensor. The results showed that this pPA–FCu nanostructure not only had excellent redox electrochemical activity, but also had good catalytic efficiency for hydrogen peroxide. Also the ZrO_2–CS–AuNPs had good film forming ability, high stability and good retention of bioactivity of the immobilized enzyme. The resulting biosensors showed a linear range from 7.80×10^{-7} to 3.7×10^{-3} mol L^{-1}, with a detection limit of 3.2×10^{-7} mol L^{-1} (S/N = 3) under optimized experimental conditions. The apparent Michaelis–Menten constant was determined to be 0.32 mM, showing good affinity. In addition, the biosensor which exhibits good analytical performance, acceptable stability and good selectivity, has potential for practical applications.

1. Introduction

The analytical determination of hydrogen peroxide plays a pivotal role in pharmaceutical, environmental, clinical and industrial research, which leads to an increasing demand for development of new methodologies for simple, rapid and reliable quantification of hydrogen peroxide. In recent years, the development of high sensitivity, high selectivity and low limit of detection amperometric biosensors based on enzyme has been proved to be the most effective tool for determination of hydrogen peroxide. In particular, biosensors which are modified with nanomaterials have recently aroused much interest. This is thanks to their high surface reaction activity, high catalytic efficiency, large surface-to-volume ratio, and strong adsorption ability [1]. In the last decade, various nanomaterials including Pt [2,3], Fe_3O_4 [4,5], copper [6], copper oxide [7,8], Ag [9], carbon nanotube [10–12], etc., have been induced to fabricate biosensors.

Among various nanomaterials, copper and copper oxide nanomaterials have recently gained increasing interest, because of their catalyzing oxidation and reduction reactions leading to sensorial, analytical, and technological applications [13–15]. Until now, many biosensors based on copper and copper oxide nanomaterials were constructed. Zhang et al. reported a sensitive non-enzymatic hydrogen peroxide sensor based on polypyrrole nanowire–copper nanocomposite [6]. Reitz et al. reported a non-enzymatic glucose sensor based on CuO nanospheres [16]. Batchelor-McAuley et al. reported the use of copper(II) oxide nanorod bundles for non-enzymatic voltammetric sensing of carbohydrates and hydrogen peroxide [17]. Umar et al. reported an enzymatic glucose biosensor based on flower-shaped copper oxide nanostructures [7]. Zhang et al. reported a non-enzymatic amperometric hydrogen peroxide biosensor based on porous cuprous oxide microcubes [8]. However, the flowerlike polymer–copper nanostructure composite (pPA–FCu) had never been used for electrochemical investigation.

Nowadays, advanced hybrid materials, especially nanoparticles enhanced hybrid materials, have been extensively used for enzyme immobilization [5,9,18,19]. This is because these interesting materials exhibit large surface-to-volume ratio, high surface reaction activity, high catalytic efficiency, and strong adsorption ability. Zirconia (ZrO_2), which is a semiconductor inorganic oxide with chemical inertness, lack of toxicity, thermal stability and affinity for the groups containing oxygen, is an ideal candidate material

* Corresponding author. Tel.: +86 23 68252277; fax: +86 23 68254000.
E-mail address: yuanruo@swu.edu.cn (R. Yuan).

0927-7765/$ – see front matter © 2009 Elsevier B.V. All rights reserved.
doi:10.1016/j.colsurfb.2009.09.015

for immobilization of biomolecules [20,21]. In addition, the ZrO_2 has intrinsic affinity for binding proteins and many literatures have indicated that proteins can be immobilized on ZrO_2 tightly. Zong et al. and Yang et al. reported immobilization of Mb and glucose oxidase in the ZrO_2 nanoparticles grafted collagen matrix and ZrO_2/CS composite film [18,19]. Zhao et al. reported immobilization of heme proteins on self-assembled ZrO_2 film and found that electrostatic interaction promoted the spontaneous adsorption of protein onto the electrode surface [22]. Chitosan (CS), derived from chitin via deacetylation with alkali, is a natural polymer product containing rich amino groups and hydroxyl groups [23]. Its excellent film forming, adhesion ability, nontoxicity together with satisfying biocompatibility have gained growing interest in biomolecule immobilization in recent years [24,25]. Gold nanoparticles (AuNPs), suitable for acting as "electronic wires", have excellent conductivity, catalytic property and good biocompatibility [26,27]. On the other hand, many works have shown that when enzymes are immobilized on gold nanoparticles, they can retain their biocatalytic and electrochemical activity [28,29]. Thus, AuNPs are particularly attractive for fabricating electrochemical biosensor. Taking into account the good performance of the ZrO_2, CS and AuNPs, an advanced hybrid material (ZrO_2–CS–AuNPs) was synthesized.

In this study, a novel hydrogen peroxide biosensor based on pPA–FCu nanostructure composite and ZrO_2–CS–AuNPs matrix was developed. First, the gold electrode was modified with pPA–FCu nanostructure composite by electrodepositing the compound of 2,6-pyridinediamine (PA) and $CuSO_4$. Then the ZrO_2–CS–AuNPs matrix, which was made up of positively charged CS hybridized, negatively charged ZrO_2 (isoelectric point is 4.15) and negatively charged AuNPs, was modified on the pPA–FCu composite. Finally, HRP was immobilized on the electrode by electrostatic interaction among ZrO_2, AuNPs and HRP. The prepared biosensor showed good analytical performance, indicating that the nanostructure pPA–FCu exhibited good redox electrochemical activity and remarkably electrocatalytic activity for H_2O_2, and the ZrO_2–CS–AuNPs matrix provided suitable microenvironment for enzyme.

2. Materials and methods

2.1. Chemicals

Horseradish peroxidase (HRP, EC 1.11.1.7, type VI), gold chloride tetrahydrate, and chitosan (CS, Mw: 100,000–300,000 g/mol, deacetylating grade: 70–85%) were purchased from Sigma Chemical Co. (St. Louis, MO, USA). 2,6-Pyridinediamine (PA) was purchased from Bailingwei Chemical Reagent Co. (Beijing, China). Zirconium oxychloride ($ZrO_2Cl_2{\cdot}8H_2O$) was purchased from Sinopharm Chemical Reagent Co. (Ltd., China). H_2O_2 (30%, m/v solution) was purchased from Shanghai Chemical Reagent Co. (Shanghai, China), and stock solutions of H_2O_2 were prepared daily. All the other reagents were analytical grade and used as received. Doubly distilled water was used throughout this study. Phosphate buffer solutions (PBS), 0.1 M at various pH were prepared by using the stock solutions of Na_2HPO_4, NaH_2PO_4, and the supporting electrolyte was 0.1 M KCl. Gold nanoparticles (AuNPs) with a diameter about 16 nm were prepared by reducing gold chloride tetrahydrate with sodium citrate at 100 °C for half an hour [30]. A stock solution of 0.5 wt% CS was prepared by dissolving 0.5 g chitosan flakes in 100 mL 1% HAc at room temperature.

2.2. Apparatus and measurements

Amperometric measurement and cyclic voltammetric experiment were performed by using a CHI 660A electrochemical work station (Shanghai Chenhua Instrument Co., China). All the electrochemical measurements were performed in the three-electrode system consisting of a modified electrode as working electrode, a Pt wire as auxiliary electrode and a saturated calomel electrode (SCE) as reference electrode. The electrochemical impedance spectroscopy (EIS) of the electrode membrane was measured with the Model IM6e (ZAHNER Elektrick, Germany). All potentials were measured versus the SCE.

UV–vis absorption spectra was recorded in the range of 200–800 nm using a type of Lambda 17 UV–VIS 8500 (PE Co., USA) with a quartz cell (path length 1 cm) at room temperature.

Scanning electron micrographs were taken with a scanning electron microscope (SEM, S-3400, Japan) at an acceleration voltage of 20 kV.

2.3. Preparation of zirconia

ZrO_2 gel was prepared according to the literature with a little modification [21]: 0.10 M $NH_3{\cdot}H_2O$ was dropped gradually into a 50.0 mL 0.01 M $ZrO_2Cl_2{\cdot}8H_2O$ solution until the pH reach to 9.5 under stirred condition. ZrO_2 gel could be seen as a white floccus throughout the dropping. The resulting ZrO_2 gel was centrifuged several times, and washed with doubly distilled water.

2.4. Preparation of ZrO_2–CS matrix

0.5 mg mL^{-1} ZrO_2–CS matrix was prepared by adding 0.5 mg ZrO_2 gel into 1 mL 0.5% CS solution. Through mixing, the corresponding solution gradually turned into milk white after stirring for some time at room temperature. This resulting milk white matrix was stored for further use.

2.5. Fabrication of hydrogen peroxide biosensor

The gold electrode (4 mm diameter) was respectively polished with 0.3 and 0.05 μm alumina slurry, and successively cleaned by sonicating in ethanol and water. pPA–FCu composite was electrodeposited onto the bare gold electrode in a solution of 0.01 mol L^{-1} PA + 0.01 mol L^{-1} $CuSO_4$ + 0.1 mol L^{-1} $NaNO_3$ (pH 5.0) by cycling between −0.8 and 1.6 V at 100 mV s^{-1} for 15 consecutive cycles. The modified gold electrode (pPA–FCu/gold electrode) was dried and then 5 μL ZrO_2–CS matrix, 5 μL AuNPs solution and 5 μL 2 mg mL^{-1} HRP solution were sequentially added onto the pPA–FCu surface to prepare the biosensor (HRP/ZrO_2–CS–AuNPs/pPA–FCu/gold electrode). For comparison, HRP/ZrO_2–CS–AuNPs/gold electrode was prepared similarly. The modified electrodes were stored above pH 6.0 PBS at 4 °C when not in use. The facturation process of the biosensor was shown in Scheme 1.

2.6. Experimental measurements

Electrochemical experiments were performed in a conventional electrochemical cell containing a three-electrode arrangement at room temperature. Cyclic voltametry (CV) was performed with a potential swept from −0.8 to 0 V (vs. SCE) under a sweeping rate of 100 mV s^{-1}. The electrochemical characteristics of the modified electrode were characterized by using impedance measurements (EIS) in presence of 10 mM $K_3[Fe(CN)_6]$/$K_4[Fe(CN)_6]$ (1:1) mixture as a redox probe in PBS (pH 6.0). The alternative voltage was 5 mV, the formal potential was 220 mV and the frequency range was 50 mHz–10 kHz.

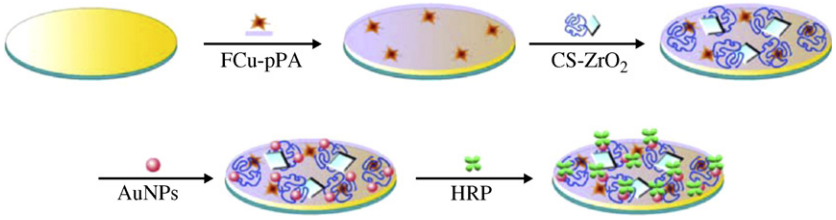

Scheme 1. Illustration of the facturation process of the biosensor.

3. Results and discussion

3.1. UV–vis analyses

The positions and shapes of the Soret absorption bands could provide information about possible denaturation of HRP proteins [31]. Fig. 1 shows UV–vis spectra of different systems. For HRP and AuNPs in PBS, the Soret bands lied at 402, 518 nm, respectively (curves a, b). All suspensions and solutions containing HRP displayed a maximum adsorption at 402 nm (curves a, d). After mixing HRP with ZrO_2–CS–AuNPs matrix (curve d), no shift of the Soret band was observable, and the reason was that the interaction between ZrO_2–CS–AuNPs matrix and HRP molecules did not change the fundamental microenvironment of HRP and did not destroy its natural secondary structure. While not all the Soret bands of AuNPs lied at 518 nm, the Soret bands shifted to 521 nm after the AuNPs solution mixed with ZrO_2–CS matrix (curves c, d). The slight shift might be due to the interaction between AuNPs and ZrO_2–CS matrix.

3.2. SEM characterization

The SEM micrographs of different membranes were shown in Fig. 2. The surface morphology of the electrodeposited copper was flowerlike and the pPA film was connected to the electrode surface (Fig. 2a). The diameter of single flower-shaped morphologies was in a range of 500–700 nm (the inset in Fig. 2a). After modified with ZrO_2–CS matrix, the surface morphology was porous, and the ZrO_2 was quadrate with an average diameter of 1 μm (Fig. 2b). After mixing AuNPs with ZrO_2–CS matrix, the AuNPs were seen dispersed inside and outside the ZrO_2–CS porous matrix (Fig. 2c).

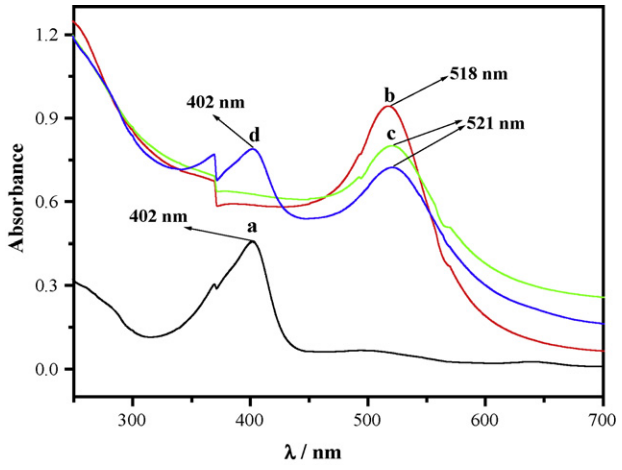

Fig. 1. UV–vis spectra of (a) HRP; (b) AuNPs; (c) ZrO_2–CS–AuNPs; (d) HRP/ZrO_2–CS–AuNPs in the PBS (pH 6.0).

3.3. Electrochemical characterization of the biosensor

EIS has been employed to characterize the interface properties of surface-modified biosensors. It is well known that the semicircle portion corresponds to the electron-transfer-limited process and the semicircle diameter in the impedance spectrum equals to the electron-transfer resistance, R_{et}. As shown in Fig. 3, the nyquist diagrams indicated almost a straight line, implying very low R_{et} on the pPA–FCu nanostructures modified electrode (Fig. 3, curve a). After ZrO_2–CS matrix was immobilized on the pPA–FCu nanostructures film, the EIS of the resulting film showed an interfacial R_{et} (Fig. 3, curve b), implying an increase of R_{et} in the redox probe. The increase was attributed to the non-conductive properties of CS and semiconductive properties of ZrO_2. The curve c of Fig. 3 showed an interfacial R_{et} of the modified electrode which was modified with pPA–FCu nanostructures and ZrO_2–CS–AuNPs matrix. Compared with curve b, a decrease of R_{et} was seen in curve c, owing to the AuNPs which played an important role similarly to a conducting wire or electron conduction tunnel. When HRP was immobilized on the ZrO_2–CS–AuNPs matrix, higher interfacial R_{et} was observed in the EIS of the resulting electrode, indicating that the non-conductive HRP was incorporated on the ZrO_2–CS–AuNPs/FCu–pPA/gold electrode.

3.4. Electrocatalytic reduction of H_2O_2 on the biosensor

The electrocatalytic behavior of HRP/ZrO_2–CS–AuNPs/pPA–FCu/gold electrode towards the electrochemical reduction of H_2O_2 was investigated by CV. Fig. 4 shows bioelectrocatalytic behavior of the hydrogen peroxide biosensor in absence (curve a) and presence of H_2O_2 (curves b and c). Upon addition of H_2O_2, a sharp increase in the cathodic current and a concomitant decrease in the anodic current were observed, showing a typical electrocatalytic reduction process of H_2O_2. Furthermore, the cathodic current increased with an increasing H_2O_2 concentration, indicating that the immobilized HRP exhibited excellent electrocatalytic activity towards the reduction of H_2O_2.

The CVs of HRP/ZrO_2–CS–AuNPs/pPA–FCu/gold electrode measured in PBS (pH 6.0) with 0.39 mM H_2O_2 at different scan rates were showed in Fig. 5. As shown in the inset of Fig. 5, the cathodic current was directly proportional to the square root of scan rate from 20 to 250 mV s^{-1}, suggesting a typical diffusion-controlled process. Hence, the response of the resulted sensor was controlled by diffusion of H_2O_2 from solution to the electrode surface.

3.5. Optimization of conditions of enzyme electrode preparation

The conditions of enzyme electrode preparation, including the electrodeposited cycle of pPA–FCu nanostructure, the concentration of ZrO_2 in the CS solution and the amount of HRP, were optimized by successive addition of 39 μM H_2O_2 at an applied potential of −300 mV. The results were shown in Fig. 6. As we could see in Fig. 6a, with the electrodeposited cycles increased from

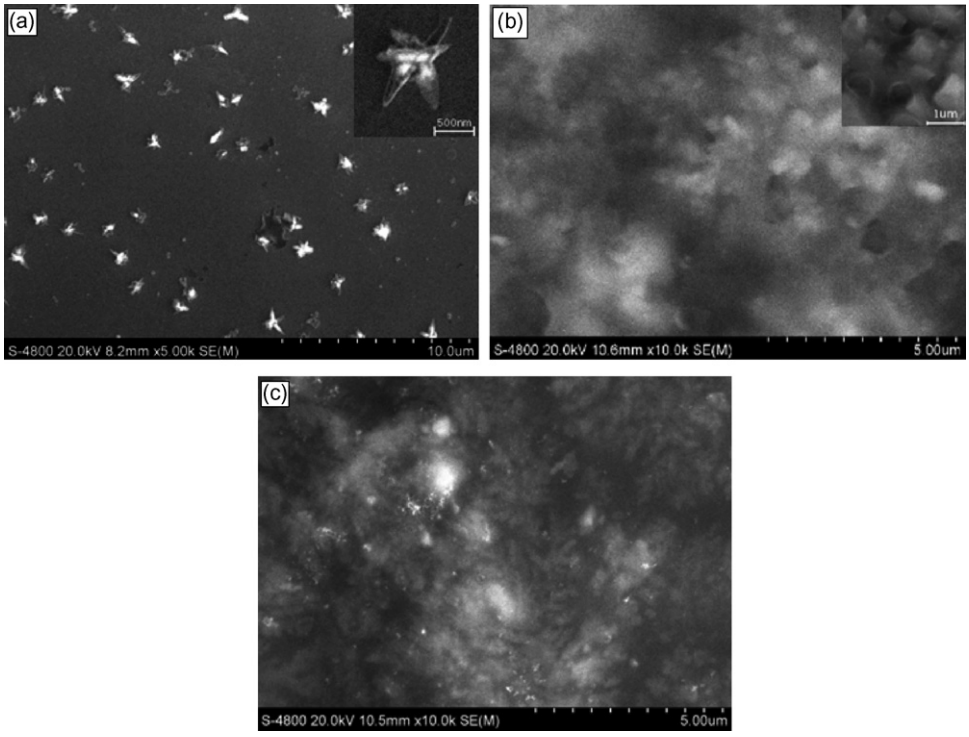

Fig. 2. SEM images of differently modified electrodes: (a) pPA–FCu/gold; (b) ZrO_2–CS/pPA–FCu/gold; (c) ZrO_2–CS–AuNPs/pPA–FCu/gold.

10 to 15, the chronoamperometric responses increased due to the larger amount of FCu formed in the pPA film. With the electrodeposited cycles increased to 20, the chronoamperometric responses decreased due to the excessive thickness of pPA–FCu composite film, which blocked the electron transfer and caused a decrease of the current response. Therefore, the electrodeposited cycles of pPA–FCu composite were 15 cycles.

Fig. 6b shows the dependence of the chronoamperometric current response to the different concentrations of the ZrO_2 in the CS solution, which are 0.5, 1.5 and 2.5 mg mL^{-1}. The maximum response of the biosensors occurred at 2.5 mg mL^{-1}, owing to the increasing ZrO_2 which resulted in more HRP loading. However, the ZrO_2–CS matrix had bad film forming ability when the concentration of ZrO_2 was 2.5 mg mL^{-1}. As a compromise, the optimal ZrO_2 concentration was 1.5 mg mL^{-1}.

As shown in Fig. 6c, the amount of HRP was investigated by 2, 5, 10 μL of 2 mg mL^{-1} HRP solution. The 5 and 10 μL had almost the same chronoamperometric responses, which corresponded to a saturated station. Hence, 5 μL of 2 mg mL^{-1} HRP solution was selected for further experiments.

3.6. Influence of pH and applied potential on biosensor response

The pH of supporting buffer solution and applied potential, which were variable in the experiment, could affect amperometric determination of H_2O_2. So the effect of pH of supporting buffer solution and the applied potential on the biosensor response was investigated by the changes of chronoamperometric current under constant hydrogen peroxide concentration (0.39 mM). As shown in

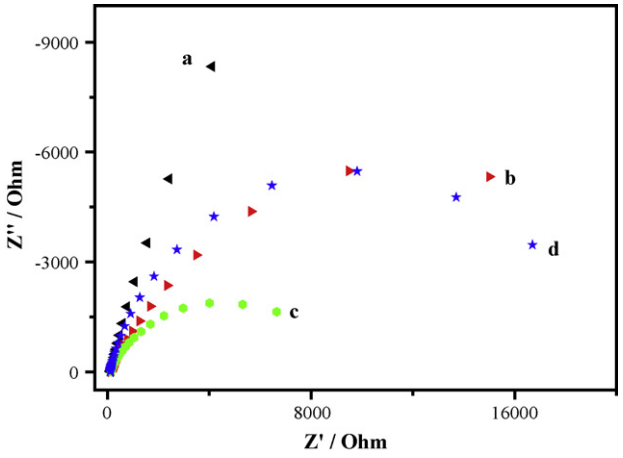

Fig. 3. EIS of the different electrodes in 10.0 mM $K_3Fe(CN)_6/K_4Fe(CN)_6$ (1:1): (a) pPA–FCu/gold; (b) ZrO_2–CS/pPA–FCu/gold; (c) ZrO_2–CS–AuNPs/pPA–FCu/gold; (d) HRP/ZrO_2–CS–AuNPs/pPA–FCu/gold.

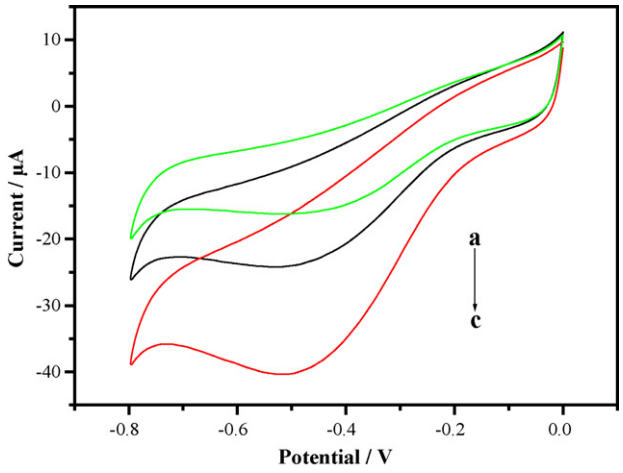

Fig. 4. CVs of HRP/ZrO_2–CS–AuNPs/pPA–FCu/gold electrode at a scan rate of 100 mV s^{-1} in 0.1 M PBS (pH 6.0) without H_2O_2 (a), with 0.39 mM H_2O_2 (b) and 1.17 mM H_2O_2 (c).

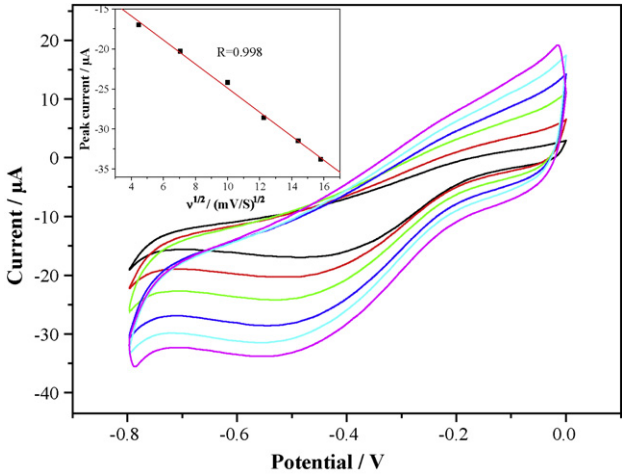

Fig. 5. CVs of HRP/ZrO_2–CS–AuNPs/pPA–FCu/gold electrode at different scan rates: 20, 50, 100, 150, 200 and 250 mV s^{-1} in 0.1 M PBS (pH 6.0). The inset shows the dependence of cathodic peak currents on the square root of scan rates.

Fig. 7a, the maximum response appeared at pH 5.5. Considering the activity of enzyme, the buffer solution of pH 6.0 was adopted for further experiments.

Fig. 7b shows the dependence of the chronoamperometric current response on the applied potential in the range from 0 V to −600 mV. As can be seen, with applied potential decreasing, the chronoamperometric current response increased due to the increased driving force for the fast reduction of H_2O_2 at the lower potentials. Considering interference of many coexisted foreign species at too negative potential, a constant potential of −300 mV was selected for amperometric measurements.

3.7. Amperometric response of hydrogen peroxide biosensor

In order to check up the electrochemical responses of different modified biosensors, a comparative study of the chronoamperometric responses for continuous addition of H_2O_2 was carried out by using two kinds of biosensor which were prepared as: (a) HRP/ZrO_2–CS–AuNPs/gold, (b) HRP/ZrO_2–CS–AuNPs/pPA–FCu/gold electrode. As shown in Fig. 8, the HRP/AuNPs–ZrO_2–CS/pPA–FCu/gold electrode showed a better chronoamperometric response than the HRP/ZrO_2–CS–AuNPs/gold. The reason was that without the aid of pPA–FCu, HRP immobilized on the hybrid film-modified gold electrode showed direct electrochemistry for its heme Fe^{III}/Fe^{II} redox couples (mechanism (1)) and the result indicated that the direct electron transfer from AuNPs–ZrO_2–CS to HRP was slow. With the aid of pPA–FCu, the obtained biosensor showed higher sensitivity, which indicated that pPA–FCu reacted as mediators could efficiently accelerate electron transfer between HRP and electrodes (mechanism (2)). The mechanisms of the bioelectrocatalytic reaction between H_2O_2 and HRP were shown as follows:

$$H_2O_2 + HRP(red) \rightarrow HRP(ox) + H_2O \quad (1)$$

$$HRP(ox) + e \rightarrow HRP(red)\,(at\ the\ electrode)$$

$$H_2O_2 + HRP(red) \rightarrow HRP(ox) + H_2O \quad (2)$$

$$HRP(ox) + pPA\text{–}FCu(I) \rightarrow HRP(red) + pPA\text{–}FCu(II)$$

$$pPA\text{–}FCu(II) + e \rightarrow pPA\text{–}FCu(I)\,(at\ the\ electrode)$$

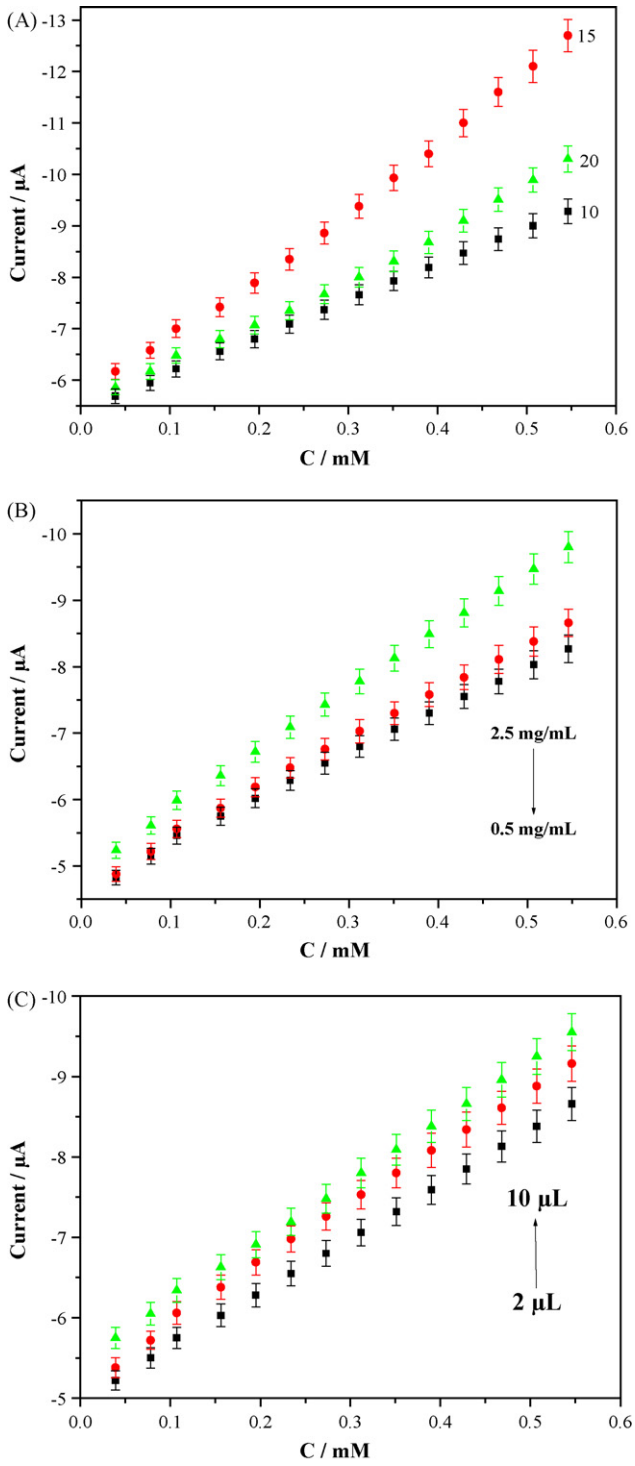

Fig. 6. Influence of conditions of enzyme electrode preparation to the amperometric response (a) the electrodeposited cycles of pPA–FCu composite; (b) the concentration of the ZrO_2 in the 0.5% CS solution; (c) the amount of the HRP.

The performance of the obtained biosensor was evaluated by detecting the concentrations of H_2O_2 under optimized conditions. The typical current–time curve and the linear calibration curve of the biosensor were shown in Fig. 9. In Fig. 9a, it was shown that the biosensor responded rapidly and could obtain about 95% of the steady-state current within 10 s. This attributed to good electron transfer of the pPA–FCu and highly porous structure of ZrO_2–CS–AuNPs matrix. Fig. 9b gave the calibration curve

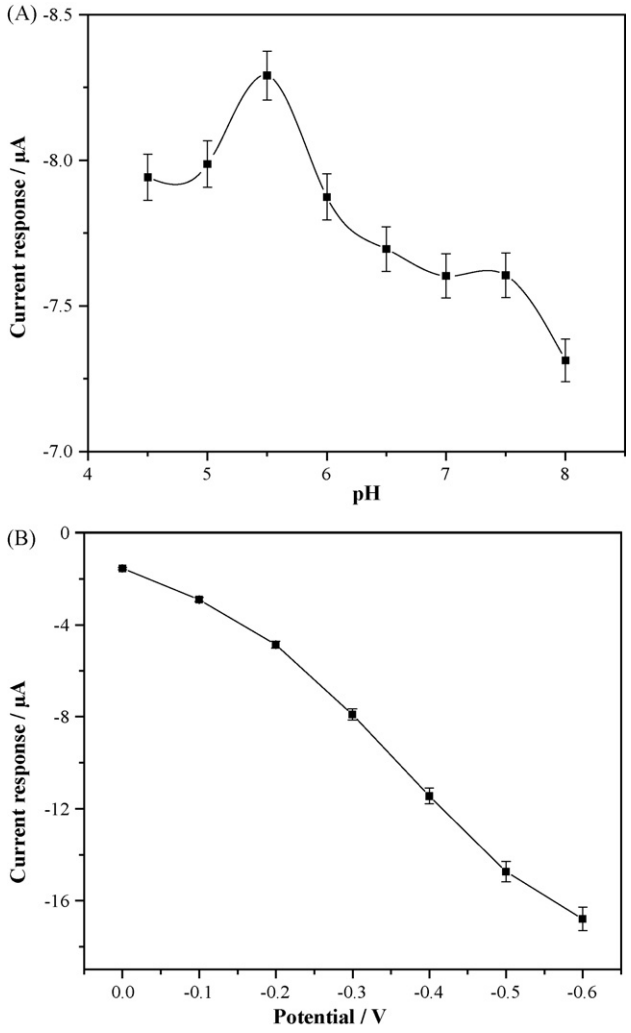

Fig. 7. Dependence of the current response of modified electrode to 0.39 mM H_2O_2 on the pH of buffer solutions at an applied potential of −300 mV (a) and on the applied potential in 0.1 M PBS (pH 6.0) (b).

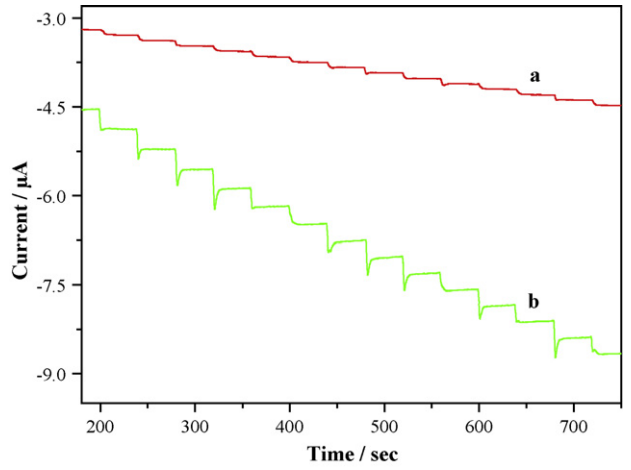

Fig. 8. Amperometric response of different electrodes to H_2O_2 in a pH 6.0 PBS at an applied potential of −300 mV upon successive addition of 0.39 mM H_2O_2 in the time intervals of 40 s. (a) HRP/ZrO_2–CS–AuNPs/gold; (b) HRP/ZrO_2–CS–AuNPs/pPA–FCu/gold.

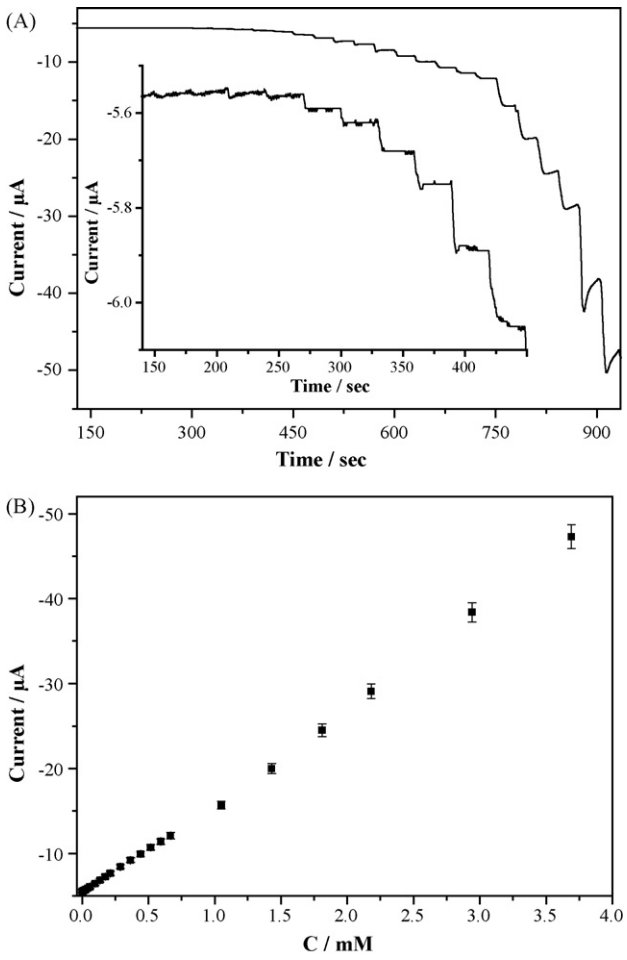

Fig. 9. Amperometric response of the biosensor to H_2O_2 at an applied potential of −300 mV in a pH 6.0 PBS (a), and the plot of steady-state current vs. H_2O_2 concentration (b).

of the biosensor, which had a linear range of H_2O_2 concentration from 7.8×10^{-7} to 3.7×10^{-3} mol L^{-1}, with a detection limit of 3.2×10^{-7} mol L^{-1} (S/N = 3). The regression equation was the form of $I/\mu A = -11.10C/mM - 5.21$, with a correlation coefficient of 0.9990.

It is well known that a smaller Michaelis–Menten constant (K_M^{app}) implies a higher catalytic activity of the immobilized enzyme. The apparent K_M^{app}, which gives an indication of the enzyme-substrate kinetics, can be calculated from the electrochemical version of the Lineweaver–Burk equation [32]: $1/I_{ss} = 1/I_{max} + K_M^{app}/I_{max}c$. Here, I_{ss} is the steady-state current after the addition of substrate; I_{max} is the maximum current measured under saturated substrate condition; c is the bulk concentration of the substrate. The K_M^{app} is determined by analyzing the slope and intercept of the plot of the reciprocals of the I_{ss} and c. The K_M^{app} of the obtained biosensor was calculated to be 0.32 mM. The value was smaller than HRP co-electrodeposited with ZrO_2 ($K_M^{app} = 8.01$) [33] and HRP bound with gold nanoparticles in the matrix of chitosan ($K_M^{app} = 4.51$) [34]. The smaller value of the K_M^{app} demonstrated that the synergistic effect between ZrO_2 and AuNPs in CS matrix had better retention of bioactivity of the immobilized HRP, which had the same result as the UV–vis analyses.

3.8. Selectivity, repeatability and stability of the biosensor

The possible interference might affect the biosensors response. It can be evaluated by the value of the current ratio, which is

Table 1
Possible interference tested with the obtained biosensor.

Potential interfering substance	Current ratio[a] (%)
Ascorbic acid	98.5 ± 1.6
Ethanol	101.5 ± 2.2
L-Threonine	104.3 ± 1.2
L-Tryptophan	103.2 ± 2.5
L-Arginine	103.8 ± 1.4
L-Cysteine	101.1 ± 2.1

[a] Mean ± SD of three measurements.

Table 2
Application of the biosensor for determining the recovery of H_2O_2.

Samples	$C_{Original}$/ μmol L^{-1}	C_{Added}/ μmol L^{-1}	C_{Found}[a]/μmol L^{-1}	Recovery %
1	3.0	5.0	8.9 ± 0.2	111.2
2	10.0	20.0	27.6 ± 0.6	95.1
3	50.0	80.0	125.1 ± 3.2	96.2
4	100.0	200.0	302.7 ± 7.9	100.9
5	500.0	600.0	1119.7 ± 13.1	101.8

[a] Mean ± SD of three measurements.

calculated from the current of 39 μM H_2O_2 with and without 2 times interferences. In our experiment, six interferences including ascorbic acid, ethanol, L-threonine, L-tryptophan, L-arginine, and L-cysteine were tested and the results were listed in Table 1. It showed that they did not cause interference in determination of H_2O_2, which was largely associated with the low working potential of −300 mV used in the experiment.

The fabrication reproducibility of six electrodes, made independently, showed an acceptable reproducibility with a R.S.D. of 6.8% for determining the same H_2O_2 concentration of 0.39 mM. When not in use, the biosensors were suspended above 0.1 M PBS in a refrigerator at 4 °C. The long-term stability of the proposed biosensor was investigated by measuring the current response of 0.39 mM H_2O_2 every 2 or 3 days over 1 month. It retained 92% of its initial current response after 1 month storage, showing the proposed biosensor possessed good stability.

3.9. Recovery experiment

To evaluate its applicability, the biosensors were used for determination the recovery of H_2O_2 by a standard addition method. The results were presented in Table 2 and the satisfying results demonstrated a great potential for practical application in analysis of H_2O_2 on real food samples.

4. Conclusion

In this study, the pPA–FCu nanostructure which had good ability to accelerate electron transfer and good ability to reduce H_2O_2 was first used in fabrication of the hydrogen peroxide biosensor. Also the ZrO_2–CS–AuNPs hybrid film which had good film forming ability and good biocompatible ability was used to improve the characteristic of the biosensor. Hence, the biosensor exhibited fast response, good affinity, wide linear range, low limit of detection, high sensitivity, good selectivity, and acceptable storage stability. More importance, this method could be used in practical applications and extended to other enzyme immobilization.

Acknowledgments

This work was supported by the National Natural Science Foundation of China (20675064), the Ministry of Education of China (Project 708073), the Natural Science Foundation of Chongqing City (CSTC-2009BA1003) and the High Technology Project Foundation of Southwest University (XSGX 02), China.

References

[1] A. Kaushik, R. Khan, P.R. Solanki, P. Pandey, J. Alam, S. Ahmad, B.D. Malhotra, Biosens. Bioelectron. 24 (2008) 676.
[2] J.J. Yu, D.L. Yu, T. Zhao, B.Z. Zeng, Talanta 74 (2008) 1586.
[3] Y.J. Zou, C.L. Xiang, L.X. Suna, F. Xu, Biosens. Bioelectron. 23 (2008) 1010.
[4] Y.X. Cheng, Y.J. Liu, J.J. Huang, K. Li, Y.Z. Xian, W. Zhang, L.T. Jin, Electrochim. Acta 54 (2009) 2588.
[5] S.F. Wang, Y.M. Tana, D.M. Zhao, G.D. Liu, Biosens. Bioelectron. 23 (2008) 1781.
[6] T.T. Zhang, R. Yuan, Y.Q. Chai, W.J. Li, S.J. Ling, Sensors 8 (2008) 5141.
[7] A. Umar, M.M. Rahman, Y.B. Hahn, Electrochem. Commun. 11 (2009) 278.
[8] L. Zhang, H. Li, Y.H. Ni, J. Li, K.M. Liao, G.C. Zhao, Electrochem. Commun. 11 (2009) 812.
[9] J.H. Lin, C.Y. He, Y. Zhao, S.S. Zhang, Sens. Actuators B 137 (2009) 768.
[10] G.D. Liu, Y.H. Lin, Electrochem. Commun. 8 (2006) 251.
[11] L.D. Zhu, R.L. Yang, J.L. Zhai, C.Y. Tian, Biosens. Bioelectron. 23 (2007) 528.
[12] X.H. Kang, Z.B. Mai, X.Y. Zou, P.X. Cai, J.Y. Mo, Anal. Biochem. 369 (2007) 71.
[13] H.Y. Liu, X.D. Su, X.F. Tian, Z. Huang, W.B. Song, J.Z. Zhao, Electroanalysis 18 (2006) 2055.
[14] J. Wang, G. Chen, M. Wang, M.P. Chatrathi, Analyst 129 (2004) 512.
[15] K.B. Male, S. Hrapovic, Y.L. Liu, D.S. Wang, J.H.T. Luong, Anal. Chim. Acta 516 (2004) 35.
[16] E. Reitz, W.Z. Jia, M. Gentile, Y. Wang, Y. Lei, Electroanalysis 20 (2008) 2482.
[17] C. Batchelor-McAuleya, Y. Du, G.G. Wildgoose, R.G. Compton, Sens. Actuators B 135 (2008) 230.
[18] S.Z. Zong, Y. Cao, Y.M. Zhou, H.X. Ju, Biosens. Bioelectron. 22 (2007) 1776.
[19] Y.H. Yang, H.F. Yang, M.H. Yang, Y.L. Liu, G.L. Shen, R.Q. Yu, Anal. Chim. Acta 525 (2004) 213.
[20] K.D. Dobson, A.J. McQuillan, Langmuir 13 (1997) 3392.
[21] S.Q. Liu, J.J. Xu, H.Y. Chen, Bioelectrochemistry 57 (2002) 149.
[22] G. Zhao, J.J. Feng, J.J. Xu, H.Y. Chen, Electrochem. Commun. 7 (2005) 724.
[23] Y.Q. Miao, S.N. Tan, Analyst 125 (2000) 1591.
[24] H. Okuma, E. Watanabe, Biosens. Bioelectron. 17 (2002) 367.
[25] X.J. Zhao, Z.B. Mai, X.H. Kanga, X.Y. Zou, Biosens. Bioelectron. 23 (2008) 1032.
[26] Q. Xu, C. Mao, N.N. Liu, J.J. Zhu, J. Sheng, Biosens. Bioelectron. 22 (2006) 768.
[27] J.B. Jia, B.Q. Wang, A.G. Wu, G.J. Cheng, Z. Li, S.J. Dong, Anal. Chem. 74 (2002) 2217.
[28] C.L. Xiang, Y.J. Zou, L.X. Sun, F. Xu, Sens. Actuators B 136 (2009) 158.
[29] S.H. Chen, R. Yuan, Y.Q. Chai, L.Y. Zhang, N. Wang, X.L. Li, Biosens. Bioelectron. 22 (2007) 1268.
[30] B.V. Enustun, J. Turkevich, J. Am. Chem. Soc. 85 (1963) 3317.
[31] B. Wang, J.J. Zhang, Z.Y. Pan, X.Q. Tao, H.S. Wang, Biosens. Bioelectron. 24 (2009) 1141.
[32] R.A. Kamin, G.S. Wilson, Anal. Chem. 52 (1980) 1198.
[33] Z.Q. Tong, R. Yuan, Y.Q. Chai, Y. Xie, S.H. Chen, J. Biotechnol. 128 (2007) 567.
[34] T. Tangkuaram, C. Ponchio, T. Kangkasomboon, P. Katikawong, W. Veerasai, Biosens. Bioelectron. 22 (2007) 2071.